THE JOURNAL OF PHYSICAL CHEMISTRY B

Article

pubs.acs.org/JPCB

Magnetic Nanoparticles for in Vivo Use: A Critical Assessment of Their Composition

Geraldo Magela da Costa,[†] Cristina Blanco-Andujar,[‡,§] Eddy De Grave,[∥] and Quentin A. Pankhurst*[,§,⊥]

[†]Chemistry Department, Federal University of Ouro Preto, Ouro Preto, Brazil

[‡]Department of Physics and Astronomy and [⊥]Institute of Biomedical Engineering, University College London, Gower Street, London, WC1E 6BT, U.K.

[§]Healthcare Biomagnetics Laboratory, University College London, 21 Albemarle Street, London, W1S 4BS, U.K.

[∥]Department of Physics and Astronomy, University of Ghent, Ghent, Belgium

ABSTRACT: Three different magnetic samples with particle sizes ranging from 10 to 30 nm were prepared by wet chemical methods. The powders were heated at 100, 150, 200, and 250 °C during 30 min under air. Ferrous and total iron contents were determined immediately after the synthesis and after the thermal treatments. All samples were characterized by X-ray diffraction, transmission and integral low-energy electron Mössbauer spectroscopy (ILEEMS) at 298 K. These samples are composed of a mixture of individual particles of maghemite and magnetite, which implies that once oxidation starts in this kind of material, it occurs throughout the entire particle volume. The existence of a maghemite/magnetite core−shell model was ruled out. A linear correlation between the average isomer shift and the magnetite content was found, allowing the estimation of the amounts of magnetite and maghemite in an unknown sample without the need of performing chemical analysis.

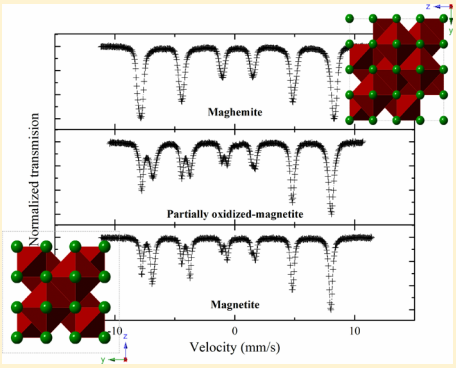

INTRODUCTION

Iron oxide nanoparticles have been extensively used for biomedical applications.[1−3] Their safety for use in biological systems has been investigated, and their short-term or long-term toxicity is a subject of continuing debate.[4] Upon cell uptake, nanoparticles are encapsulated in endocytic organelles where degradation and incorporation into the metabolic cell cascade occurs.[5,6] However, the oxidation state of the iron in these nanoparticles is not generally considered, the toxicity studies commonly having been carried out on so-called "iron oxide nanoparticles" without assessing whether magnetite or maghemite is used. As a rule of thumb, it is accepted that magnetite nanoparticles are examined; however, nanosized magnetite is known to naturally oxidize, at least partly, toward maghemite, thus leading to an unknown composition of the tested product.[7] Furthermore, it is important to consider that after cell uptake and decomposition, magnetite nanoparticles can release Fe^{2+} in solution, which may incur undesirable side effects due to the catalytic production of reactive oxygen species (ROS) (eqs 1 and 2 hereafter).[8] Additionally, the naturally occurring superoxide radical ($\bullet O_2^-$), can react with Fe^{3+} to produce Fe^{2+} and enhance the catalytic Haber−Weiss reaction (eq 3 hereafter).[9,10] The superoxide radical is produced both intra- and extracellularly by cell lines such as phagocytes or endothelial cells, among others.[11] As a result, the possible toxicity considerations do have a direct effect independently of the application or target of the nanoparticles.

$$Fe^{2+} + H_2O_2 \rightarrow Fe^{3+} + OH^- + OH^\bullet \quad (1)$$

$$Fe^{3+} + H_2O_2 \rightarrow Fe^{2+} + OOH^\bullet + H^+ \quad (2)$$

$$Fe^{3+} + \bullet O_2^- \rightarrow Fe^{2+} + O_2 \quad (3)$$

Biological systems do have in place enzymatic pathways to scavenge unwanted naturally occurring radical species such as the superoxide dismutase (SOD), which is extremely efficient and neutralizes the superoxide radicals. Additionally, SOD generally inhibits the generation of radicals from the reaction of Fe^{3+} with H_2O_2.[12] However, the presence of nanoparticles in a biological system may produce additional stress caused by the generation of new ROS and thus alter the redox equilibrium inside the cells, leading to toxicity. Bare iron oxide nanoparticles were found to be considerably toxic at high concentrations (2.5−5 nM) on lung cancer cells (A549) and HeLa cells, with an increase of ROS production and subsequent toxicity after 96 h.[13] Interestingly, a similar study was carried out on A549 upon exposure to 100 μg/mL of iron oxide nanoparticles: the results showed a 10-fold increase of ROS after 24 h, which was toxic for cancer cells; while noncancerous cells viability was not altered significantly.[14] On the other hand, the ROS production on astrocytes exposed to iron oxide nanoparticles was found to initially increase but return to basal level after 3 days with no significant changes in viability.[15] Together these reports illustrate the fact that the effect of the

Received: June 5, 2014
Revised: July 31, 2014
Published: September 11, 2014

dx.doi.org/10.1021/jp5055765 | J. Phys. Chem. B 2014, 118, 11738−11746

presence of Fe^{2+} in cells is not yet fully understood and thus a deeper knowledge of the composition of the used material is needed before we can truly ensure stability and controlled behavior of iron oxide nanoparticles once they are introduced into biological entities.

Several different methods of synthesis and coating of the magnetic particles have been described in the literature, and Mössbauer spectroscopy has played an important role in the characterization of these materials. However, we believe that in many cases the interpretation of the Mössbauer spectra might not be entirely correct because the possible presence of maghemite might have been disregarded.

The room-temperature Mössbauer spectra of well-crystallized maghemite ($Fe^{3+}[Fe^{3+}_{5/3}\square_{1/3}]O_4$), magnetite ($Fe^{3+}[Fe^{2+}Fe^{3+}]O_4$), and a partially oxidized magnetite ($Fe^{3+}[Fe^{2+}_{0.82}Fe^{3+}_{1.12}\square_{0.06}]O_4$) made at 1300 °C in a controlled O_2 partial pressure are displayed in Figure 1 ($\square$ stands for

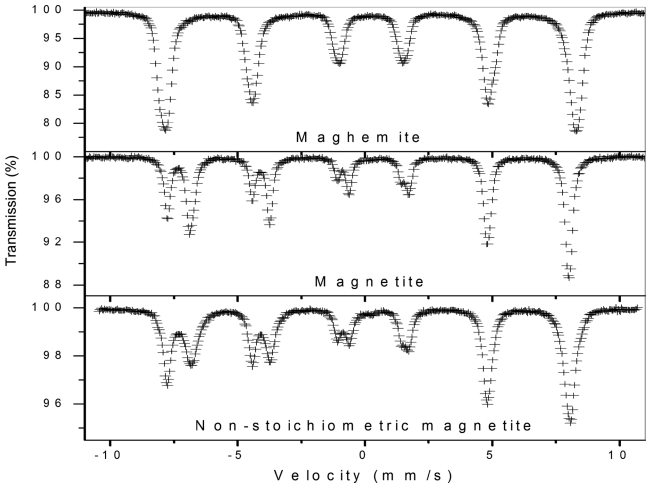

Figure 1. Room-temperature Mössbauer spectra of well-crystallized maghemite, magnetite, and partially oxidized magnetite.

vacancies). The area ratio of the inner sextet versus that of the outer sextet in the spectrum of magnetite is close to 1.9 and decreases with increasing deviation from stoichiometry, that is, increasing degree of oxidation. In this case the area ratio $r_{AB} = S_A/S_B$ of the A-site Mössbauer sextet to that for the B-site often deviates significantly from the ideal value of 0.52 for pure stoichiometric magnetite as dictated by the equation:

$$\frac{S_A}{S_B} = r_{AB} = \frac{f_A}{f_B}\frac{n_A}{n_B} = 1.05\frac{n_A}{n_B} \tag{4}$$

in which n_I is the number of iron species on site I and f_I is the recoil free fraction for that site (fraction of iron, in general, contributing to the spectrum). In some cases, this deviation can be interpreted as a partial oxidation of the magnetite. Partial oxidation means that, in contrast to ideal Fe_3O_4, the B sublattice contains more Fe^{3+} than Fe^{2+}. The excess ferric irons (y) must be compensated by the presence of neutral vacancies ($\square$), because the species must stay electrically neutral. This reasoning then leads to the chemical composition:

$$Fe^{3+}_A[Fe^{3+}_y(Fe^{3+}_xFe^{2+}_x)\square_{2-2x-y}]_BO_4 \tag{5}$$

where pure maghemite corresponds to $x = 0$ and $y = {}^5/_3$, and pure magnetite corresponds to $x = 1$ and $y = 0$.

A magnetite molecule will be electrically neutral if the total charge of the cations within the [ ] is 5+:

$$3y + 3x + 2x = 5x + 3y = 5 \tag{6}$$

As a result of the fast electron hopping, the (Fe^{2+}, Fe^{3+}) pairs produce the low-field ($H_{hf} \approx 460$ kOe) component in the room temperature magnetite spectrum. The remaining Fe^{3+} species on the B sites (y p.f.u.) generate a subspectrum that generally cannot be resolved from the A-site subspectrum, having a hyperfine field of ~490 kOe. Therefore, in a quantitative analysis concerning partially oxidized magnetite, the alleged A-site-component's spectral area will be more or less grossly overestimated due to the contribution of the unpaired octahedral Fe^{3+} cations to the A-site subspectrum. Considering this reasoning, the ratio n_A/n_B in eq 4, instead of being 0.5 as for stoichiometric magnetite, should be taken as $(1 + y)/2x$, and hence one obtains:

$$r_{AB} = 1.05\frac{n_A}{n_B} = 1.05\frac{Fe^{3+}_A + Fe^{3+}_y}{Fe^{3+}_x + Fe^{2+}_x} = 1.05\frac{1+y}{2x} \tag{7}$$

From eqs 6 and 7, one can then calculate the quantities x and y. Finally, the Fe^{2+}/Fe^{3+} ratio ε in the partially oxidized magnetite phase is given by

$$\varepsilon = \frac{x}{1+x+y} \tag{8}$$

Although the spectra shown in Figure 1 seem to be quite different, it is not possible to distinguish these phases if they exist in a mixture. This fact is due to the complete overlap of the A-site contribution of magnetite with the two unresolvable sextets of maghemite. Small-particle sizes result in line broadening, but the essential feature of the spectrum of magnetite, that is, the existence of two clearly resolved sextets, is preserved. All this information has long been known and was well documented in the 1970s and 1980s literature.[16−18] However, in recent years a large number of papers have appeared associating the broad envelope of maghemite to magnetite. Several examples of this doubtful interpretation will be presented hereafter.

The use of X-ray diffraction to differentiate these three iron-oxide phases is also ineffective because they possess the same cubic structure with nearly equal unit-cell parameters. Thus, in this work attention was focused on the well-known dichromate titrimetric method to quantify Fe^{2+} in magnetic nanoparticles which subsequently enabled the derivation of a correlation between the Mössbauer spectrum and the amount of Fe^{2+} in these kinds of materials.

EXPERIMENTAL SECTION

Three different magnetic samples were prepared by the following methods: (i) Sample Ca7, ferric chloride was reduced by sodium sulphite;[19] (ii) Sample Ca8, ferrous sulfate mixed with KOH and KNO_3;[20] (iii) Sample Ca10, similar to CA8 but with different proportions of reactants.[21,22]

Samples Ca7, Ca8, and Ca10 were heated at 100, 150, 200, and 250 °C during 30 min under air. Ferrous and total iron contents were determined immediately after the synthesis and after the thermal treatments. To this purpose, the potassium dichromate method (~0.0036 mol·L^{-1}) was used after dissolving about 50 mg of the samples in warm concentrated HCl. The crucial step here was to titrate as quickly as possible to minimize Fe^{2+} spontaneous oxidation in air.

dx.doi.org/10.1021/jp5055765 | J. Phys. Chem. B 2014, 118, 11738−11746

Mössbauer absorbers were prepared immediately, although the spectra were collected some days later. The absorbers were covered with a layer of Styrofoam previously dissolved in benzene to prevent any further spontaneous oxidation at room temperature. The effectiveness of this measure was confirmed by also collecting the spectra 30 days after the respective initial runs, and within the experimental errors no alterations were observed.

Transmission Mössbauer spectra were collected at room temperature (298 K) with a time-mode spectrometer using a constant-acceleration drive with triangular reference signal. Data were accumulated in 1024 channels (unfolded) covering a velocity range of approximately −11 to +11 mm/s, with a velocity increment of ∼0.045 mm/s per channel. The velocity was calibrated from the Mössbauer spectrum of a standard α-Fe foil at room temperature. The spectra were computer-fitted either with model-independent distributions of magnetic hyperfine fields and quadrupole splittings or with discrete sextets.[23,24]

X-ray diffraction (XRD) patterns were collected in a Shimadzu XRD 6000 diffractometer equipped with an iron tube (Fe Kα) and a graphite monochromator. The scans were done between 20 and 60° (2θ) with a scanning speed of 1°/min and step-size of 0.02°. Patterns were fitted with a Pearson function after subtraction of the background and the Kα2 contribution. Cell parameters of the magnetic phases were calculated using angular and intensity weighting of the peaks located at ∼38, 45, and 55°. Particle sizes were estimated from the Scherrer equation.

Simulated patterns (Fe Kα) based on line intensities and positions were produced for mixtures of maghemite (PDF card 39-1346) and magnetite (PDF card 19-0629) using the relative intensity ratios (RIR) given in their PDF files: 1.4 for maghemite and 4.9 for magnetite. For these simulations low (3000) and high (300000) intensity (I) counts were considered, and the fluctuation of the data was modeled as dev = $(9 \times (\text{random} - 0.5) \times I^{1/2})$. The effect of small (15 nm) and large particle-sizes (150 nm) was also simulated. A Pearson VII function was used, with a step size of 0.02° and inclusion of the Kα2 contribution. Data analysis and simulation were done with the software Jade from Materials Data Inc.

RESULTS AND DISCUSSION

Characterization. The XRD patterns of samples Ca7, Ca8, and Ca10 are very similar (Figure 2) and could be indexed both with maghemite (PDF card 39-1346) and magnetite (PDF card 19-0629). The estimated particle sizes are 10 nm (Ca7), 40 nm (Ca8), and 30 nm (Ca10). As discussed below, is it not possible to distinguish between maghemite and magnetite by XRD, and hence at this point all that can be concluded is that magnetic iron oxide nanoparticles have been obtained.

Total ferric and ferrous contents in the original and heated samples, as determined using the potassium dichromate method, are shown in Table 1. Magnetite contains 24.1 wt % Fe^{2+}, and therefore none of the Ca samples can be considered to be pure magnetite, as the ferrous contents are lower than the above value. The amounts of magnetite and maghemite in these samples are estimated assuming that all Fe^{2+} belongs to magnetite and no other Fe-bearing phases are present. Thus:

$$\text{magnetite (wt \%)} = 4.14 \times \text{Fe}^{+2}\text{(wt \%)}$$

$$\text{Fe}_{\text{total}}\ \text{(in magnetite)} = 3 \times \text{Fe}^{+2}\text{(wt \%)}$$

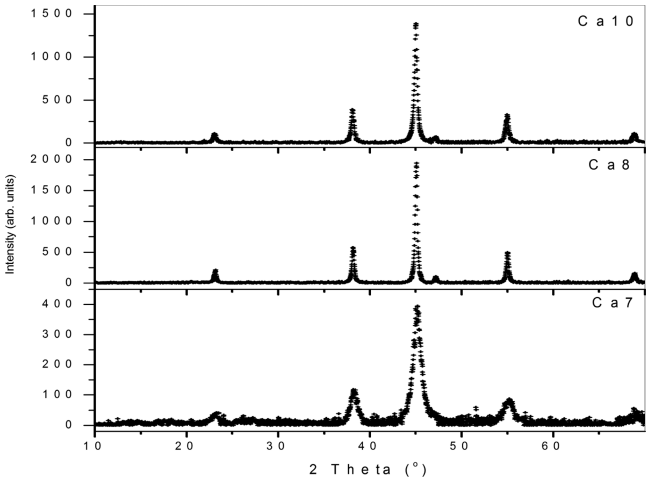

Figure 2. X-ray diffraction patterns of samples Ca7 (bottom), Ca8 (middle), and Ca10 (top).

Table 1. Ferrous, Ferric, Magnetite and Maghemite Contents (wt %) in the As-Prepared and Heated Samples. Absolute Errors for Fe^{2+} and Fe_{total} are 0.5 wt %

sample	Fe^{2+}	Fe^{3+}	Fe^{2+}/Fe^{3+}	Fe_{total}	magnetite	maghemite
Ca7	8.6	56.0	0.15	64.6	39.1	60.9
Ca7-100	5.6	59.0	0.095		25.3	74.7
Ca7-150	0.34	64.3	0.0053		1.5	98.5
Ca7-200	0.39	64.2	0.0060		1.7	98.3
Ca7-250	0.08	64.6	0.0012		0.3	99.7
Ca8	19.4	51.9	0.37	71.3	81.1	18.9
Ca8-100	18.6	52.7	0.35		77.7	22.3
Ca8-150	7.9	63.4	0.12		32.5	67.5
Ca8-200	7.3	64.0	0.11		30.0	70.0
Ca8-250	0.47	70.8	0.0066		2.0	98.0
Ca10	18.3	52.4	0.35	70.7	77.1	22.9
Ca10-100	16.6	54.1	0.31		69.7	30.3
Ca10-150	6.5	64.2	0.10		29.7	70.3
Ca10-200	2.5	68.2	0.037		10.3	89.7
Ca10-250	0.04	70.7	0.0006		0.2	99.8

$$\text{Fe}^{3+}\ \text{(maghemite)} = \text{Fe}_{\text{total}} - 3 \times \text{Fe}^{2+}\text{(wt \%)}$$

$$\begin{aligned}\text{maghemite (wt \%)} &= [\text{Fe}_{\text{total}} - 3 \times \text{Fe}^{2+}\text{(wt \%)}]/(2 \times 55.85/159.7) \\ &= 1.43[\text{Fe}_{\text{total}}\text{(wt \%)} - 3\text{Fe}^{2+}\text{(wt \%)}]\end{aligned}$$

The results of these calculations were normalized to 100 wt % and are included in Table 1. The total iron contents in the heated samples were assumed to be the same as those of the original samples.

X-ray Diffraction. Simulated patterns for 15 nm maghemite, magnetite, and some mixtures of them are shown in Figure 3. All patterns are similar, except for those materials containing 60, 80, and 100 wt % of maghemite, in which a few additional weak lines are found between 30 and 35° (2θ). However, experimental patterns normally show a much more pronounced scatter in their background, and hence these lines are hardly seen in the patterns of poorly crystallized maghemite. After simulation, each pattern was fitted using one peak modeled by a Pearson VII function for each reflection. The cubic cell parameters a were subsequently calculated using

dx.doi.org/10.1021/jp5055765 | J. Phys. Chem. B 2014, 118, 11738−11746

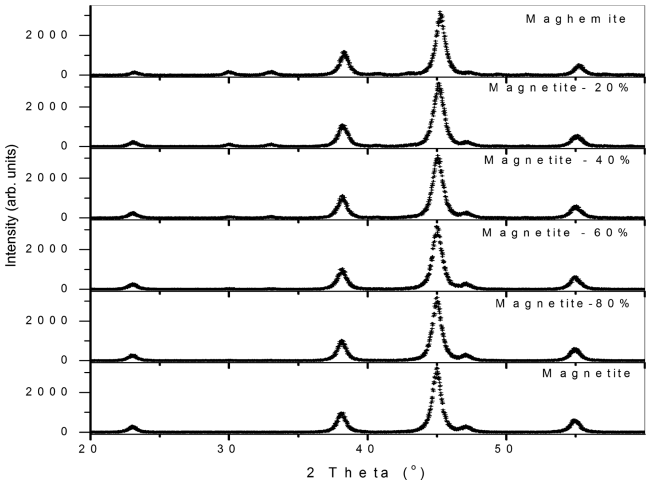

Figure 3. Simulated XRD patterns of 15 nm maghemite, magnetite, and mixtures of them.

angular and intensity weighting of the five peaks of highest intensity.

A correlation between the cell parameters and the composition of the system is depicted in Figure 4. A nonlinear relationship is observed, which shows that the usual assumption of a linear decrease of the cell parameter in going from magnetite to maghemite is not correct.

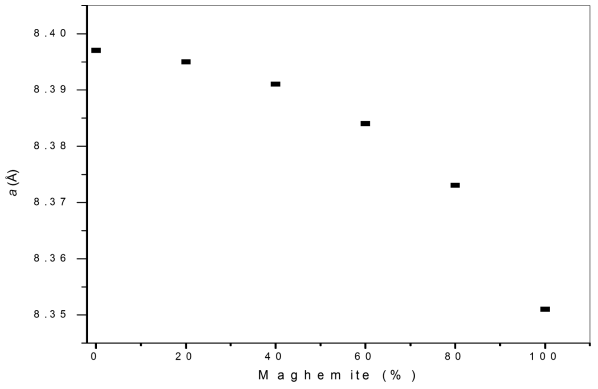

Figure 4. Variation of the cell parameters of 15 nm magnetite-maghemite mixtures as a function of the maghemite content.

The effect of the particle size on the calculation of the cell parameter of maghemite is shown in Figure 5, in which the patterns were simulated for particle sizes of 150 nm. A mixture of 60 wt % maghemite and 40 wt % magnetite shows at $2\theta >$ 40° the presence of peaks of both phases, which allows the calculation of the cell parameter of maghemite without significant influence of the magnetite peaks. Under these conditions, a value of ~8.358 Å was found for the simulation with low (3000) as well as high (300 000) counts, which was in agreement with the reference value (PDF card 39-1346). The obtained cell parameter for the same composition with 15 nm particles (Figure 4) was 8.384 Å. The difference is easily explained as in Figure 4 the plotted values refer to the cell parameter of the whole sample, and not only maghemite.

Real samples, however, normally do not present such narrow lines as used in these simulations (0.10° 2θ), meaning that in the vast majority of cases there is no separation of the maghemite and magnetite diffraction lines. Therefore, X-ray

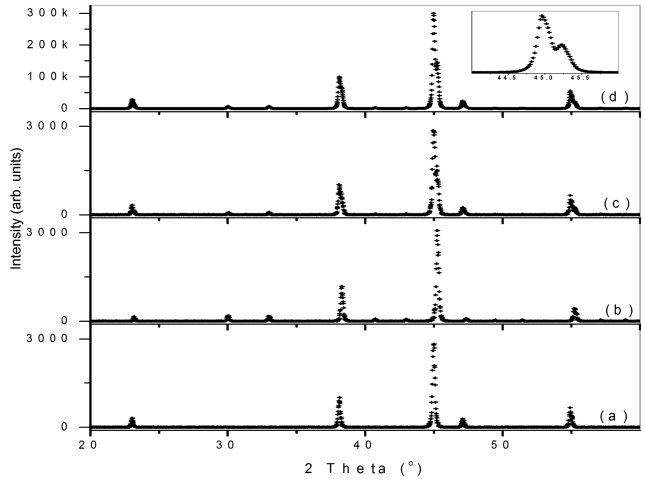

Figure 5. Simulated XRD patterns of 150 nm magnetite (a), maghemite (b), and of a mixture of 60 wt % maghemite and 40 wt %. The inset shows the separation of the main peaks of magnetite (45.0°) and maghemite (45.2°).

diffraction is definitely not an appropriate tool to confirm the possible presence of maghemite (or magnetite) in this type of sample.

Mössbauer Spectroscopy. The transmission Mössbauer spectra of all the samples are shown in Figures 6, 7, and 8, and

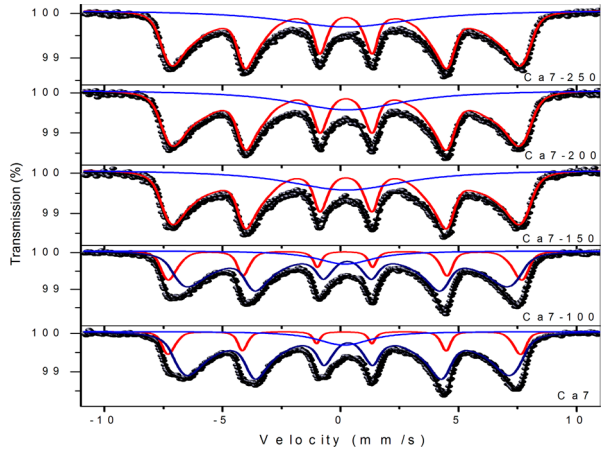

Figure 6. Transmission Mössbauer spectra (298 K) of Ca7 samples.

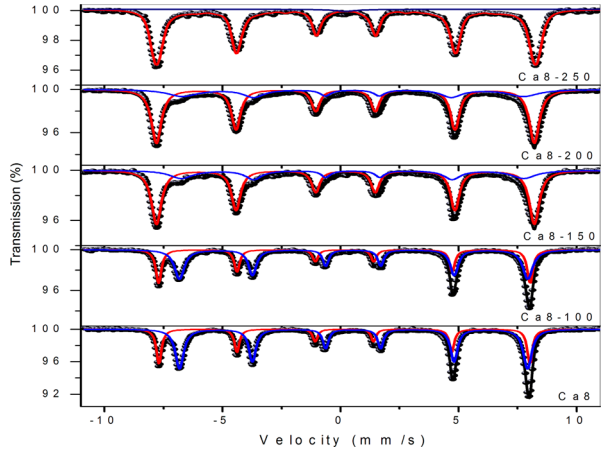

Figure 7. Transmission Mössbauer spectra (298 K) of Ca8 samples.

dx.doi.org/10.1021/jp5055765 | J. Phys. Chem. B 2014, 118, 11738−11746

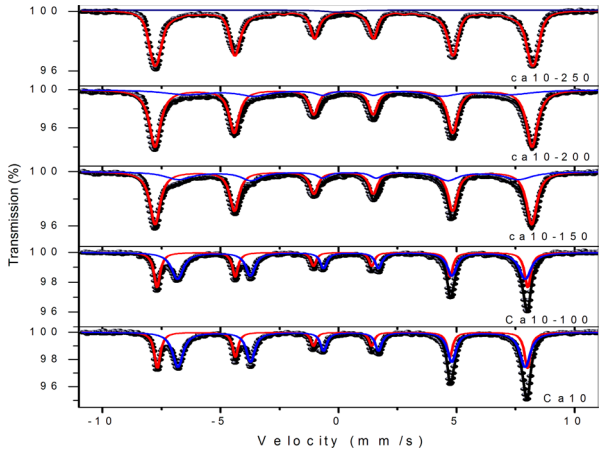

Figure 8. Transmission Mössbauer spectra (298 K) of Ca10 samples.

relevant numerical data derived from the fits are given in Table 2. All Ca7 samples show one broad asymmetric sextet and attempts to fit Ca7 and Ca7−100 with only one hyperfine-field distribution (HFD) component failed. Reasonable fits of these spectra were obtained using superpositions of two distributed sextet components and one quadrupole-splitting distribution (QSD). For the first sextet component the hyperfine field was allowed to vary within the range from 400 to 500 kOe with a step of 5 kOe. The quadrupole shift was fixed at 0 mm/s and the line area ratios at 3:2:1. The initial value for the isomer shift was chosen to be 0.26 mm/s. For the second sextet the field ranged from 150 to 470 kOe with a step of 10 kOe. As for the first sextet component the quadrupole shift was fixed at 0 mm/s and the area ratios were set at 3:2:1. The initial value for the isomer shift was input as 0.66 mm/s. For the QSD the quadrupole splitting of the symmetric doublet ranged between 0.2 and 1.0 mm/s with a step of 0.1 mm/s. As seen in Figure 6, this procedure resulted in an adequate description of the experimental line shapes, and the derived Mössbauer parameters for the sextet components (Table 2) seem to have physically meaningful values. It should be emphasized that the results for the broad central envelope, which was modeled as a doublet, are likely to be unrealistic. Moreover, it remains unclear as to which Fe phase this broad central absorption is due. The adjusted isomer shift values are indicative of the 6-fold coordinated Fe^{3+} species, but more specific details cannot be inferred.

It is tempting to correlate the outer and inner sextets with the A- and B-sites of magnetite, respectively. However, the hyperfine fields are significantly lower than in pure magnetite. Another crucial parameter in this respect is the isomer shift derived for the inner sextet (~0.45 mm/s), which is drastically lower than the value commonly found for magnetite, that is, 0.66 mm/s.[16,18,25] Thus, despite exhibiting two sextets in their Mössbauer spectra, samples Ca7 and Ca7-100 cannot be regarded as pure magnetite, as could actually already be expected on the basis of their low Fe^{2+} contents.

The transmission Mössbauer spectra of sample Ca7 heated at 150, 200, and 250 °C were adjusted with one HFD (range from 200 to 520 kOe, step of 10 kOe, line intensities 3:2:1 and quadrupole splitting fixed at 0 mm/s) and one QSD (fitted as described above). Some misfits are obvious, but considering the complexity of these spectra the fits may be considered as acceptable. The absence of a second sextet in these experimental line shapes is no proof for the absence of magnetite because the B-site contribution of the latter could be hidden by the broad sextet component and therefore totally unresolved, especially if the magnetite phase would be present as a minor constituent. On the other hand, the obtained parameters (Table 2) suggest maghemite to be the dominant Fe oxide in the involved samples.[26−28] Hence, materials which present Mössbauer spectra that are similar to those of samples Ca7, or that show the S_A/S_B area ratio significantly different from 0.52 (eq 4), cannot be considered as being magnetite, in contrast to what is claimed in several papers that have been published.[29−43]

Two sextets are clearly seen in the transmission Mössbauer spectra of the Ca8 and Ca10 samples heated at temperatures of up to 200 °C (Figures 7 and 8), but not even the spectra of the as-prepared unheated samples closely resemble the Mössbauer spectrum of pure magnetite (Figure 1). As compared to the latter, the lowering of the peak depths of the outer negative-velocity absorption lines of the inner sextet is noticeable, especially when going from the sample heated at 100 °C to that

Table 2. Hyperfine Parameters Derived from Fitting the Room-Temperature Mössbauer Spectra[a]

sample	H_{hf1}	δ_1	S_1	H_{hf2}	δ_2	S_2	S_1/S_2	ΔE_Q	δ	S
Ca7	464	0.27	13	429	0.44	77	0.17	0.5	0.28	10
Ca7-100	466	0.30	22	428	0.40	68	0.32	0.5	0.31	10
Ca7-150	459	0.34	73					0.7	0.36	27
Ca7-200	459	0.34	74					0.7	0.39	26
Ca7-250	460	0.34	74					0.8	0.34	26
Ca8	487	0.27	35	457	0.65	65	0.54			
Ca8-100	488	0.28	39	458	0.66	61	0.64			
Ca8-150	500	0.32	73	450	0.62	27	2.70			
Ca8-200	497	0.32	72	448	0.62	28	2.57			
Ca8-250	498	0.34	99					0.4	0.32	1
Ca10	487	0.28	37	456	0.65	63	0.59			
Ca10-100	487	0.28	40	457	0.65	60	0.66			
Ca10-150	495	0.32	71	447	0.55	29	2.45			
Ca10-200	496	0.32	74	426	0.51	26	2.85			
Ca10-250	497	0.34	99					0.4	0.3	1

[a] H_{hf} is the maximum-probability hyperfine field (kOe), δ is the isomer shift relative to α-Fe (mm/s), ΔE_Q is the maximum-probability quadrupole splitting (mm/s), and S is the relative area (%).

dx.doi.org/10.1021/jp5055765 | J. Phys. Chem. B 2014, 118, 11738−11746

heated at 150 °C. The spectra for the samples heated at temperatures of up to 200 °C could be adequately fitted using superpositions of two discrete Lorentzian-shaped sextets, and the derived hyperfine fields and isomer shifts (Table 2) are similar to those of magnetite.[18] However, the A- to B-site relative area ratios differ from those of stoichiometric magnetite, indicating that these samples are either a mixture of magnetic phases or that they consist of partially oxidized magnetite.

The transmission Mössbauer spectra of samples Ca8-250 and Ca10-250 were fitted with only one HFD (range from 200 to 520 kOe, step of 10 kOe, line intensities 3:2:1 and quadrupole splitting fixed at 0 mm/s) and one QSD (fitted as described above). The obtained values of the hyperfine parameters suggest that maghemite is the main iron phase present in these samples.[26−28]

As discussed above, it is possible that some samples such as Ca8-100 contain partially oxidized magnetite instead of a mixture of magnetite and maghemite. The numerical results for x and y and for the Fe^{2+}/Fe^{3+} ratios ε as calculated from the Mössbauer parameters S_1 (= S_A) and S_2 (= S_B) are listed in Table 3. It is clear that the values of the calculated ferrous to

Table 3. Parameters Derived from the Mössbauer Spectra Considering the Samples To Consist of Partially Oxidized Magnetite: $Fe_A^{3+}\,[Fe_y^{3+}(Fe_x^{3+}Fe_x^{2+})\square_{2-2x-y}]_BO_4$

sample	x	y	ε
Ca7	1.33	−0.56	
Ca7-100	1.17	−0.29	
Ca7-150			
Ca7-200			
Ca7-250			
Ca8	0.99	0.017	0.49
Ca8-100	0.92	0.13	0.45
Ca8-150	0.39	1.02	0.16
Ca8-200	0.41	0.99	0.17
Ca8-250			
Ca10	0.96	0.073	0.47
Ca10-100	0.91	0.15	0.44
Ca10-150	0.42	0.97	0.18
Ca10-200	0.38	1.04	0.16
Ca10-250			

ferric ratios ε are significantly different from those obtained by chemical analysis (Table 1). In addition, negative values for y imply that the model is not correct; hence, the possibility that the involved samples are single-phase partially oxidized magnetites can most probably be ruled out, and these samples rather consist of mixtures of magnetite and maghemite. Of course, the possibility of the existence of three-component systems cannot be excluded and in that case quantitative conclusions about the compositions can neither be derived from their Mössbauer spectra nor from chemical analyses.

Recently Salazar et al. reported a study of the properties of nanoparticles of ferrimagnetic iron oxides in terms of the magnetite/maghemite molar ratio.[44] They propose that the larger (>20 nm) particles have a core−shell structure, consisting of a magnetite core surrounded by a maghemite-like shell layer. They described their room-temperature Mössbauer spectra with a magnetic HFD with the isomer-shift value of the elemental sextet components being correlated to their hyperfine field. The mean stoichiometry of their samples, that is, the molecular fractions of magnetite and maghemite, was estimated from the evaluated mean isomer shift, thereby assuming specific values of the isomer shifts for octahedral and tetrahedral Fe^{3+} and for octahedral Fe^{2+}. However, it is not clearly described in their paper how the calculations were exactly carried out, and the estimated compositions were not compared with results of chemical analyses of the respective ferrous contents.

Building on the idea of Salazar et al., we have calculated the mean isomer shifts δ_{aver} of the investigated samples as

$$\delta_{aver} = \frac{1}{100}\sum \delta_i S_i \tag{9}$$

where δ_i and S_i are the isomer shifts and relative area ratios (in %), respectively, of all components resolved from the corresponding Mössbauer spectra. The variation of δ_{aver} with the magnetite contents (Table 1) is shown in Figure 9. A

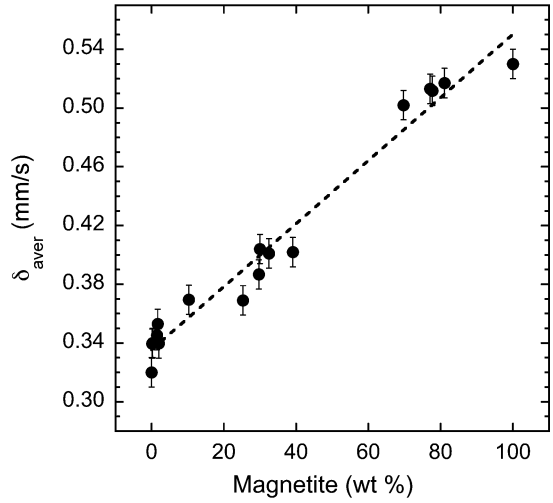

Figure 9. Correlation between the mean isomer shifts and the magnetite contents determined by chemical analysis.

constant error of 0.01 mm/s for δ_{aver} was assumed, and data points referring to the average isomer shifts of maghemite (0 wt % Fe^{2+}) and magnetite (24.1 wt % Fe^{2+}), that is, 0.32 and 0.53 mm/s, respectively, are included in the plot. A nearly linear correlation is obtained and can be expressed as

$$\delta_{aver}(\text{mm/s}) = 0.335 + 0.00215 \times \text{magnetite (wt \%)} \quad (r^2 = 0.97) \tag{10}$$

From this equation the amount of magnetite present in a magnetite/maghemite mixture can be estimated. However, with an error of 0.01 mm/s in the δ_{aver} values, the uncertainty in the magnetite content will be of the order of 5 wt %. In view of the fairly complicated line shapes of the Mössbauer spectra, it is believed that the estimated error of 0.01 mm/s for δ_{aver} is not unrealistic as it can be expected that different fitting approaches (e.g., different upper and/or lower limits for the HFDs, smaller or lower step values, etc.) might possibly produce slightly different values for δ_{aver}. Despite the relatively large uncertainty in the magnetite content, eq 10 is useful to estimate the amounts of magnetite and maghemite in an unknown sample without the need to perform chemical analysis.

As mentioned above, the room-temperature transmission Mössbauer spectra of our samples as well as those reported in

dx.doi.org/10.1021/jp5055765 | J. Phys. Chem. B 2014, 118, 11738−11746

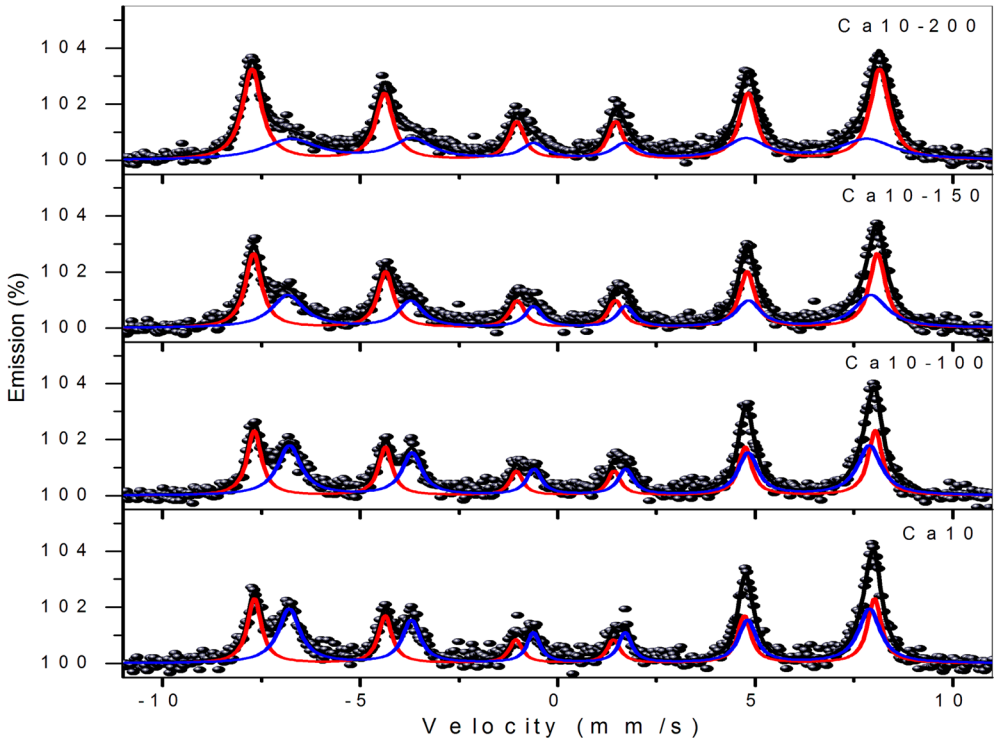

Figure 10. ILEEMS Mössbauer spectra (298 K) of Ca10 samples.

Table 4. Hyperfine Parameters Derived from Fitting the Room-Temperature Transmission (TMS) and ILEEMS Mössbauer Spectra[a]

sample		H_{hf1}	$\Gamma_{1,6}$	δ_1	S_1	H_{hf2}	$\Gamma_{1,6}$	δ_2	S_2	δ_{aver}
Ca10-fresh	(TMS)	489	0.29	0.28	36	459	0.56	0.66	64	0.52
Ca10-5weeks	(TMS)	490	0.36	0.28	42	460	0.60	0.66	58	0.50
	(ILEEMS)	487	0.42	0.28	44	456	0.66	0.66	56	0.49
Ca10-100	(TMS)	490	0.36	0.28	42	460	0.62	0.66	58	0.50
	(ILEEMS)	488	0.43	0.29	44	455	0.73	0.66	56	0.50
Ca10-150	(TMS)	494	0.47	0.30	55	460	0.92	0.65	44	0.45
	(ILEEMS)	490	0.49	0.31	54	458	1.00	0.66	46	0.47
Ca10-200	(TMS)	498	0.55	0.32	69	454	1.34	0.61	31	0.41
	(ILEEMS)	493	0.59	0.32	60	452	1.68	0.65	40	0.45

[a] H_{hf} is hyperfine field (kOe), δ is the isomer shift relative to α-Fe (mm/s), $\Gamma_{1,6}$ is the full-width at half maximum of lines 1 and 6 (mm/s), and S is the relative area (%). The average isomer shift (mm/s) is given by δ_{aver}.

the literature for similar materials show a strong superposition of the A- and B-site sextets. Several authors have obtained the transmission Mössbauer spectra at 77 K in an attempt to better resolve these two sextets. However, we believe that this procedure is impractical in the sense that it does not provide any new information regarding the composition and magnetic behavior of these materials. The 77 K Mössbauer spectrum may show a different shape when compared to the 298 K spectrum, but this is not a conclusive proof for the existence of magnetite, maghemite, nor partially oxidized magnetite.[16,17,22,45−47]

The maghemite/magnetite core−shell model has been invoked by almost all researchers to explain the composition of materials similar to the present samples. However, to the best of our knowledge, no conclusive proofs have been presented so far regarding this core−shell model. In an attempt to clarify this issue, we have collected ILEEMS spectra for some samples. ILEEMS stands for integral low-energy electron Mössbauer spectroscopy, a variant that counts the low-energy resonant electrons that are predominantly emitted by Fe species located in a surface layer of a few nanometers thickness.[48,49] Therefore, if the ILEEMS reveals different parameters compared to those of the transmission spectrum, then the surface layer has indeed a different composition from that of the inner part of the particle. The reverse is also true, that is, if both spectra have the same parameters, then the sample might be composed of individual particles of two different phases.

ILEEMS and transmission spectra of a new batch of Ca10, Ca10-100, Ca10-150, and Ca10-200 samples were collected during the same period of time. As the transmission spectra of the samples of this second batch are identical to those shown in Figure 8, only their ILEEMS data are shown in Figure 10. The preparation of Ca10 was carried-out in Brazil, but the ILEEMS spectra were collected in Belgium 5 weeks later, and unfortunately no ILEEMS spectrum of the freshly prepared sample is available. It is interesting to note that a significant alteration of the relative area ratios occurred after this five-week lapse of time, indicating a partial oxidation of the sample at

dx.doi.org/10.1021/jp5055765 | J. Phys. Chem. B 2014, 118, 11738−11746

ambient conditions. All spectra were fitted with two discrete Lorentzian-shaped sextets and the numerical results are displayed in Table 4. The hyperfine fields, isomer shifts, and relative area ratios are the same, within experimental errors, for both transmission and emission spectra. This is of course also true for the average isomer shift. On the other hand, the line widths of both sextets are broader in the ILEEMS spectra as the surface layer is more defective than the core. Another observation is that the line widths for the inner sextet are much broader than the widths of the outer sextet. For the sample heated at 200 °C, the value is 1.68 mm/s, a value much larger than the natural line width. These broader lines reflect the heterogeneity of the particles compositions and structural defects. Therefore, small differences in the line widths caused by different fitting procedures will cause variations in the relative area ratios of the two sextets. For this reason it is believed that the transmission and emission parameters are the same even for sample Ca10-200.

In terms of particle compositions, as mentioned above, the existence of partially oxidized magnetite could already be ruled out. Hence, the next plausible proposition would be the core−shell model. However, as the ILEEMS results turned out to be the same as those from the transmission spectra, this core−shell model is also unlikely to be real. Thus, it is proposed that this kind of material essentially consists of individual particles of maghemite and magnetite, which implies that once oxidation starts, it occurs throughout the entire particle volume. Most methods to synthesize iron oxides make use of heterogeneous precipitation, implying the formation of particles with a relatively broad particle-size distribution. In the case of magnetite, the oxidation process is known to occur more easily in the smallest particles leading to the formation of maghemite.

CONCLUSIONS

The synthesis or storage of magnetite nanoparticles under air atmosphere results in partial oxidation, and as a consequence maghemite is also formed. The results of this work have proven that the investigated samples are composed of individual particles of both magnetite and maghemite. The core−shell model that is invoked in literature to explain the composition of these particles was found to be unrealistic for the present samples. A linear correlation between the average isomer shift and the magnetite content was found, allowing the estimation of the amounts of magnetite and maghemite in an unknown sample without the need to perform chemical analysis.

AUTHOR INFORMATION

Corresponding Author

*E-mail: q.pankhurst@ucl.ac.uk. Tel: +44 (0)20 3108 1124.

Notes

The authors declare no competing financial interest.

ACKNOWLEDGMENTS

This work was partially funded by CNPq (Brazil) and FWO (Belgium).

REFERENCES

(1) Pankhurst, Q. A.; Thanh, N. K. T.; Jones, S. K.; Dobson, J. Progress in Applications of Magnetic Nanoparticles in Biomedicine. *J. Phys. D, Appl. Phys.* **2009**, *42*, 224001.

(2) Barreto, J. A.; O'Malley, W.; Kubeil, M.; Graham, B.; Stephan, H.; Spiccia, L. Nanomaterials: Applications in Cancer Imaging and Therapy. *Adv. Mater.* **2011**, *23*, H18−H40.

(3) Gupta, A. K.; Gupta, M. Synthesis and Surface Engineering of Iron Oxide Nanoparticles for Biomedical Applications. *Biomaterials* **2005**, *26*, 3995−4021.

(4) Singh, N.; Jenkins, G. J. S.; Asadi, R.; Doak, S. H. Potential Toxicity of Superparamagnetic Iron Oxide Nanoparticles (SPION). *Nano Rev.* **2010**, *1*, 5358−5373.

(5) Gu, L.; Fang, R. H.; Sailor, M. J.; Park, J. H. In Vivo Clearance and Toxicity of Monodisperse Iron Oxide Nanocrystals. *ACS Nano* **2012**, *6*, 4947−4954.

(6) Wang, J. A.; Pantopoulos, K. Regulation of Cellular Iron Metabolism. *Biochem. J.* **2011**, *434*, 365−381.

(7) Jolivet, J. P.; Chaneac, C.; Tronc, E. Iron Oxide Chemistry. From Molecular Clusters to Extended Solid Networks. *Chem. Commun.* **2004**, 481−487.

(8) Brillas, E.; Sirés, I.; Oturan, M. A. Electro-Fenton Process and Related Electrochemical Technologies Based on Fenton's Reaction Chemistry. *Chem. Rev.* **2009**, *109*, 6570−6631.

(9) Haber, F.; Weiss, J. Über die Katalyse des Hydroperoxydes. *Naturwissenschaften* **1932**, *20*, 948−950.

(10) McCord, J. M.; Day, E. D., Jr. Superoxide-Dependent Production of Hydroxyl Radical Catalyzed by Iron-EDTA Complex. *FEBS Lett.* **1978**, *86*, 139−142.

(11) Afanas'ev, I. B. *Superoxide Ion: Chemistry and Biological Implications*; CRC Press: Boca Raton, FL, 1989; Vol. *1*.

(12) Gutteridge, J. M. C. Superoxide Dismutase Inhibits the Superoxide-Driven Fenton Reaction at Two Different Levels: Implications for a Wider Protective Role. *FEBS Lett.* **1985**, *185*, 19−23.

(13) Malvindi, M. A.; De Matteis, V.; Galeone, A.; Brunetti, V.; Anyfantis, G. C.; Athanassiou, A.; Cingolani, R.; Pompa, P. P. Toxicity Assessment of Silica Coated Iron Oxide Nanoparticles and Biocompatibility Improvement by Surface Engineering. *PLoS One* **2014**, *9*, 1−11.

(14) Khan, M. I.; Mohammad, A.; Patil, G.; Naqvi, S. A. H.; Chauhan, L. K. S.; Ahmad, I. Induction of ROS, Mitochondrial Damage and Autophagy in Lung Epithelial Cancer Cells by Iron Oxide Nanoparticles. *Biomaterials* **2012**, *33*, 1477−1488.

(15) Geppert, M.; Hohnholt, M. C.; Nürnberger, S.; Dringen, R. Ferritin Up-Regulation and Transient ROS Production in Cultured Brain Astrocytes after Loading with Iron Oxide Nanoparticles. *Acta Biomater.* **2012**, *8*, 3832−3839.

(16) Murad, E.; Johnston, J. H. Iron Oxides and Oxyhydroxides. In *Mössbauer Spectroscopy Applied to Inorganic Chemistry*; Long, G. J., Ed.; Plenum Press: New York, 1987; p 507−582.

(17) Vandenberghe, R. E.; De Grave, E. Mössbauer Effect Studies of Oxidic Spinels. In *Mössbauer Spectroscopy Applied to Inorganic Chemistry*; Long, G. J., Grandjean, F, Eds.; Plenum Press: New York, 1989; p 59−182.

(18) Rosenberg, M.; Frank, H. Mössbauer Spectroscopy of Magnetite and Related Compounds. *Philos. Mag.* **1980**, *42*, 419−421.

(19) Qu, S.; Yang, H.; Ren, D.; Kan, S.; Zou, G.; Li, D.; Li, M. Magnetite Nanoparticles Prepared by Precipitation from Partially Reduced Ferric Chloride Aqueous Solutions. *J. Colloid Interface Sci.* **1999**, *215*, 190−192.

(20) Schwertmann, U.; Cornell, R. M. *Iron Oxides in the Laboratory*; VCH: Weinheim, Germany, 1991.

(21) Sugimoto, T.; Matijevic, E. Formation of Uniform Spherical Magnetite Particles by Crystallization of Ferrous Hydroxide Gels. *J. Colloid Interface Sci.* **1980**, *74*, 227−243.

(22) da Costa, G. M.; De Grave, E.; de Bakker, P. M. A.; Vandenberghe, R. E. Influence of Nonstoichiometry and the Presence of Maghemite on the Mössbauer Spectrum of Magnetite. *Clays Clay Miner.* **1995**, *43*, 656−668.

(23) Vandenberghe, R. E.; De Grave, E.; de Bakker, P. M. A. On the Methodology of the Analysis of Mössbauer Spectra. *Hyperfine Interact.* **1994**, *83*, 29−49.

(24) Vanderberghe, R. E.; Barrero, C. A.; da Costa, G. M.; Van San, E.; De Grave, E. Mössbauer Characterization of Iron Oxides and (Oxy) hydroxides: The Present State of the Art. *Hyperfine Interact.* **2000**, *126*, 247−259.
(25) Daniels, J. M.; Rosencwaig, A. Mössbauer Spectroscopy of Stoichiometric and Nonstoichiometric magnetite. *J. Phys. Chem. Solids* **1969**, *30*, 1561−1571.
(26) Armstrong, J. R.; Morrish, A. H.; Sawatzky, G. A. Mössbauer Study of Ferric ions in Tetrahedral and Octahedral Sites of a Spinel. *Phys. Lett.* **1966**, *23*, 414−416.
(27) Annersten, H.; Hafner, S. S. Vacancy Distribution in Synthetic Spinels of the Series Fe_3O_4-γ-Fe_2O_3. *Z. Kristallogr.* **1973**, *137*, 321−340.
(28) Haneda, K.; Morrish, A. H. On the Hyperfine Field of γ-Fe_2O_3 Small Particles. *Phys. Lett.* **1977**, 259−262.
(29) Roca, A. G.; Marco, J. F.; del Puerto Morales, M.; Serna, C. J. Effect of Nature and Particle Size on Properties of Uniform Magnetite and Maghemite Nanoparticles. *J. Phys. Chem. C* **2007**, *111*, 18577−18584.
(30) Belessi, V.; Zboril, R.; Tucek, J.; Mashlan, M.; Tzitzios, V.; Petridis, D. Ferrofluids from Magnetic-Chitosan Hybrids. *Chem. Mater.* **2008**, *20*, 3298−3305.
(31) Gan, Z. F.; Jiang, J. S.; Yang, Y.; Du, B.; Qian, M.; Zhang, P. Immobilization of Homing Peptide on Magnetite Nanoparticles and its Specificity in Vitro. *J. Biomed. Mater. Res.-A* **2008**, *84*, 10−18.
(32) Andrade, A. L.; Souza, D. M.; Pereira, M. C.; Fabris, J. D.; Domingues, R. Z. pH Effect on the Synthesis of Magnetite Nanoparticles by the Chemical Reduction−Precipitation Method. *Quim. Nova* **2010**, *33*, 524−527.
(33) Li, D.; Teoh, W. Y.; Djunaedi, D.; Gooding, J. J.; Selomulya, C.; Amal, R. Facile Functionalization and Phase Reduction Route of Magnetic Iron Oxide Nanoparticles for Conjugation of Matrix Metalloproteinase. *Adv. Eng. Mater.* **2010**, *12*, B210−B214.
(34) Martinelli, J. R.; Sene, F. F.; Kamikawachi, C. N.; Partiti, C. S. M.; Cornejo, D. R. Synthesis and Characterization of Glass-Ceramic Microspheres for Thermotherapy. *J. Non-Cryst. Solids* **2010**, *356*, 2683−2688.
(35) Oshtrakh1, M. I.; Rodriguez, A. F. R.; Semionkin, V. A.; Santos, J. G.; Milder, O. B.; Silveira, L. B.; Marmolejo, E. M.; Ushakov, M. V.; de Souza-Paris, M.; Morais, P. C. Magnetic Fluid: Comparative Study of Nanosized Fe_3O_4 and Fe_3O_4 Suspended in Copaiba Oil Using Mössbauer Spectroscopy with a High Velocity Resolution. *J. Phys. Conf. Ser.* **2010**, *217*, 012018.
(36) Paulino, A. T.; Guilherme, M. R.; Mattoso, L. H. C.; Tambourgi, E. B. Smart Hydrogels Based on Modified Gum Arabic as a Potential Device for Magnetic Biomaterial. *Macromol. Chem. Phys.* **2010**, *211*, 1196−1205.
(37) Santos, J. G.; Silveira, L. B.; Ferreira, Q. S.; Garg, V. K.; Oliveira, A. C.; Parise, M. S.; Morais, P. C. The Stability of Magnetic Colloid Based from Copaiba Oil. *J. Phys. Conf. Ser.* **2010**, 214012133.
(38) Paulino, A. T.; Fajardo, A. R.; Junior, A. P.; Muniz, E. C.; Tambourgi, E. B. Two-step Synthesis and Properties of a Magnetic-Field-Sensitive Modified Maltodextrin-Based Hydrogel. *Polym. Int.* **2011**, *60*, 1324−1333.
(39) Dutta, R. K.; Sahu, S.; Reddy, V. R. Synthesis, Characterization, and in Vitro Release of Diclofenac Sodium from Hybrid Nanostructured Magnetite−Calcium Pectinate. *J. Nanopart. Res.* **2012**, *14*, 1052−1066.
(40) Kalska-Szostko, B.; Rogowska, M.; Dubis, A.; Szymański, K. Enzymes Immobilization on Fe_3O_4−Gold Nanoparticles. *Appl. Surf. Sci.* **2012**, *258*, 2783−2787.
(41) Silva, V. A. J.; Andrade, P. L.; Silva, M. P. C.; Bustamante, A. D.; De Los SantosValladares, L.; Aguiar, J. A. Synthesis and Characterization of Fe_3O_4 Nanoparticles Coated with Fucan Polysaccharides. *J. Magn. Magn. Mater.* **2013**, *343*, 138−143.
(42) Oshtrakh, M. I.; Šepelákc, V.; Rodriguez, A. F. R.; Semionkin, V. A.; Ushakov, M. V.; Santos, J. G.; Silveira, L. B.; Marmolejo, E. M.; De Souza Parisef, M.; Morais, P. C. Comparative Study of Iron Oxide Nanoparticles As-Prepared and Dispersed in Copaiba Oil Using Mössbauer Spectroscopy with Low and High Velocity Resolution. *Spectrochim. Acta, Part A* **2013**, *100*, 94−100.
(43) Zélis, P. M.; Pasquevich, G. A.; Stewart, S. J.; Fernández van Raap, M. B.; Aphesteguy, J.; Bruvera, I. J.; Laborde, C.; Pianciola, B.; Jacobo, S.; Sánchez, F. H. Structural and Magnetic Study of Zinc-Doped Magnetite Nanoparticles and Ferrofluids for Hyperthermia Applications. *J. Phys. D Appl. Phys.* **2013**, *46*, 1−12.
(44) Salazar, J. S.; Perez, L.; de Abril, O.; Phuoc, L. T.; Ihiawakrim, D.; Vazquez, M.; Grenèche, J. M.; Begin-Colin, S.; Pourroy, G. Magnetic Iron Oxide Nanoparticles in 10−40 nm Range: Composition in Terms of Magnetite/Maghemite Ratio and Effect on the Magnetic Properties. *Chem. Mater.* **2011**, *23*, 1379−1386.
(45) da Costa, G. M.; Laurent, Ch.; De Grave, E.; Vandenberghe, R. E. A Comprehensive Mössbauer Study of Highly Substituted Aluminum Maghemites. *Geochem. Soc., Special Pub.* **1996**, *5*, 93−104.
(46) da Costa, G. M.; De Grave, E.; Bowen, L. H.; de Bakker, P. M. A.; Vandenberghe, R. E. Variable-Temperature Mössbauer Spectroscopic Study of Nano-Sized Maghemite and Al-substituted Maghemites. *Clays Clay Miner.* **1995**, *43*, 562−568.
(47) Gorski, C. A.; Scherer, M. M. Determination of Nanoparticulate Magnetite Stoichiometry by Mössbauer Spectroscopy, Acidic Dissolution, and Powder X-ray Diffraction: A Critical Review. *Am. Mineral.* **2010**, *95*, 1017−1026.
(48) De Grave, E.; Vandenberghe, R. E.; Dauwe, C. ILEEMS: Methodology and Applications to Iron Oxides. *Hyperfine Interact.* **2005**, *161*, 147−160.
(49) Nedkov, I.; Merodiiska, T.; Slavov, L.; Vandenberghe, R. E.; Kusano, Y.; Takada, J. Surface Oxidation, Size and Shape of Nano-Sized Magnetite Obtained by Co-precipitation. *J. Magn. Magn. Mater.* **2006**, *300*, 358−367.